Wave numbers and pressure-induced shifts of Ar I atomic lines measured by Fourier transform spectroscopy

2012 J. Phys. B: At. Mol. Opt. Phys. 45 115001

(http://iopscience.iop.org/0953-4075/45/11/115001)

IOP PUBLISHING JOURNAL OF PHYSICS B: ATOMIC, MOLECULAR AND OPTICAL PHYSICS

J. Phys. B: At. Mol. Opt. Phys. **45** (2012) 115001 (11pp) doi:10.1088/0953-4075/45/11/115001

Wave numbers and pressure-induced shifts of Ar I atomic lines measured by Fourier transform spectroscopy

Damir Veza[1], **Craig J Sansonetti, Marc L Salit and John C Travis**

National Institute of Standards and Technology, Gaithersburg, MD 20899, USA

E-mail: veza@phy.hr

Received 8 March 2012, in final form 16 April 2012

Abstract

Wave numbers and pressure-induced shifts of 19 blue argon emission lines belonging to the $3p^5 6p$–$3p^5 4s$ and $3p^5 5p$–$3p^5 4s$ transition arrays were measured with high accuracy using a UV/visible Fourier transform spectrometer (FTS). The measurements were made using electrodeless lamps containing traces of ^{198}Hg and argon at pressures of 33 Pa (1/4 Torr), 400 Pa (3 Torr), 933 Pa (7 Torr) and 1333 Pa (10 Torr). Calibration of the FTS wave number scale was obtained using the four most prominent lines of ^{198}Hg as internal standards. The pressure-induced shifts of the argon emission lines are in reasonable agreement with theoretical predictions. These results are of importance for astronomers and analytical chemists who use argon lines for practical wavelength standards as well as for theoreticians calculating argon–argon interactions and potential energy curves of diatomic argon molecules.

1. Introduction

The spectra of neutral and singly-ionized argon have been extensively studied over many decades [1–6]. Naturally occurring argon is composed of 99.600% ^{40}Ar, 0.337% ^{36}Ar and 0.063% ^{38}Ar. Since these even isotopes have nuclear spin $I = 0$, the spectral lines of Ar are free of magnetic hyperfine structure. Thanks to the dominance of ^{40}Ar, they are also essentially free of isotope splitting. Because argon has many sharp spectral lines and is easily excited in a variety of simple light sources, it has traditionally been used by astronomers as a source of practical wavelength standards. Values for the energy levels of the $3p^5 4s$, $3p^5 4p$ and $3p^5 5p$ configurations were adopted by Commission 14 of the International Astronomical Union at the 1955 Assembly [7], and $3p^5 5s$ and $3p^5 3d$ levels at the 1964 Assembly [8]. These level values, which were recommended for use in calculating Ritz wavelength standards, were based on the best interferometric measurements of that time [1, 2, 9]. Today, in applications such as constraining cosmological variations in the fundamental constants from quasar absorption lines, wavelength calibration using argon lines is crucial since correct interpretation of the astronomical data depends on the wavelength calibration accuracy [10].

In analytical chemistry applications, the atmospheric-pressure inductively coupled plasma (ICP) discharge sustained in argon is regularly applied to determine the chemical composition of a sample with which the plasma is seeded [11]. Of analytical importance are the spectral lines of elements from the material to be analysed; the wavelengths indicate which elements are present in the sample and the intensities deliver information about their concentrations. However, in addition to the lines of analytically important elements, the ICP spectra contain argon carrier gas lines. In many experiments the argon lines are used as reference lines (e.g. for glow discharge optical emission spectroscopy [12]). They may also interfere with analytical spectral lines when they have nearly the same wavelength. In either case, whether as interfering or reference lines, accurate wavelengths are needed for the argon lines that are present in the spectrum.

Three comprehensive Ar I line lists exist with similar wavelength precision: Norlén [4], Li and Humphreys [3] and Whaling *et al* [6]. Norlén's atlas contains both Ar I and Ar II lines whereas [3, 6] contain Ar I lines only. Whaling has presented an Ar II line list of comparable accuracy in [5].

---

[1] Permanent address: Physics Department, Faculty of Science, University of Zagreb, Zagreb, Croatia.

Fewer lines are listed by Norlén than by Li and Humphreys or Whaling *et al* because Norlén's experiment was less sensitive to weak lines. The three experiments were performed under different source conditions, most significantly with different argon pressures in the light sources. Since atomic line positions are sensitive to the carrier gas pressure, knowledge of pressure-induced shifts is needed to account for this effect. Unfortunately, measurements of the collisional shift and broadening of Ar I atomic lines belonging to the $3p^56p$–$3p^54s$ and $3p^55p$–$3p^54s$ transition arrays (blue lines) are scarce. We are aware of two experiments in which the pressure broadening and shift of only three lines belonging to these transition arrays were studied [13, 14].

Aeschliman *et al* [13] report measurements of the pressure shift and broadening constants for 14 lines of neutral argon. They observed emission from a variable-pressure direct-current discharge using a plane, pressure-scanned Fabry–Pérot interferometer. The source was run with flowing argon at a pressure of 0.266–10.64 kPa (2–80 Torr) with a discharge current of 3–15 mA. The discharge temperature was kept in the range of 350–400 K. In this study 13 of the 14 lines investigated belong to the $3p^54p$–$3p^54s$ transition array (red lines), and the blue line at 416 nm was the only one belonging to the $3p^55p$–$3p^54s$ system. Bielski *et al* [14] report pressure shift and broadening constants for three argon lines from the $3p^56p$–$3p^54s$ (360.6 nm), $3p^55p$–$3p^54s$ (430 nm), and $3p^54p$–$3p^54s$ (667.7 nm) transition arrays. The light source was a water-cooled glow discharge tube, kept at a constant temperature of 310 K. Light was collected from the positive column of the glow discharge, with gas pressure between 66 and 2400 Pa (0.5 and 18 Torr) at a discharge current of 1.5 mA. The lines were analysed using a pressure scanned Fabry–Pérot interferometer with a photomultiplier in the photon counting mode.

The purpose of this paper is to present new measurements of wave numbers and pressure-induced shifts of Ar I lines belonging to the blue $3p^56p$–$3p^54s$ and $3p^55p$–$3p^54s$ transition arrays. In contrast to the $3p^54p$–$3p^54s$ transition array, which has been extensively studied for decades, the experimental and theoretical shift and broadening parameters for the blue lines are not known. In section 2 we describe our experimental setup and the method of measurement. Section 3 is devoted to presentation and discussion of our measured wave numbers and pressure-induced shifts, comparison of our data with the results of other experiments, and discussion of the calculation of pressure shifts of argon lines. In section 4 we present conclusions based on our measurements and calculations.

2. Experiment

The results reported in this paper are derived from the same spectra used previously to measure argon-induced pressure shifts in ^{198}Hg [15]. The experimental setup, data acquisition, and evaluation process are identical to the ones described in connection with that work [15, 16] and will be discussed only briefly.

The spectra were excited in low pressure electrodeless discharge lamps (EDL) filled with a few mg of ^{198}Hg and pure argon. Two nominally identical sealed lamps were prepared at each of four fixed pressures of argon: 33 Pa (1/4 Torr), 400 Pa (3 Torr), 933 Pa (7 Torr) and 1333 Pa (10 Torr) [16]. The lamps were excited in an Evenson cavity [17] with microwave power at a frequency of 2450 MHz and were water cooled to a temperature of (8 ± 0.5) °C. At this temperature the argon working pressure was about 4% lower than the nominal filling pressure, and the mercury vapour pressure was about 50 mPa (≈0.4 mTorr) [18].

A Fourier transform spectrometer (FTS), optimized for operation in the violet and ultraviolet (UV) regions [19], was used to observe the spectra. The lamp was mounted directly in front of the entrance aperture of the FTS, uniformly illuminating the aperture. The spectrum was recorded several times for each lamp in the UV (250–450 nm) and visible (380–650 nm) spectral ranges, with a typical resolution of 0.03 cm^{-1}.

In our spectra the FTS instrumental function and Doppler broadening dominate the observed line profiles, strongly masking any collisional contribution to the widths. Consequently, analysis of these spectra cannot deliver reliable collisional line-widths and pressure broadening rates. Shift rates, however, can be determined accurately because the line positions are not affected by the symmetric broadening attributable to the FTS instrumental function or Doppler effect.

The positions of the observed lines in the spectra were determined by fitting a model line profile constructed as the convolution of a Gaussian and a sinc function, which is the instrumental function of the FTS. The position, intensity, and both sinc and Gaussian widths were treated as adjustable parameters. The fits were made using a standard nonlinear least squares routine that returned optimized values and asymptotic standard deviations for each of the parameters.

3. Results and discussion

3.1. Wave numbers

Although spectra measured with a FTS are highly linear in wave number, a multiplicative correction must be made to obtain an absolute wave number scale [11, 16]. This correction was derived from the 546.2, 436.0, 404.8 and 365.1 nm lines of ^{198}Hg, which served as internal standard lines. Their wave numbers were determined with high accuracy (relative standard uncertainty of about 1.2×10^{-8}) with respect to Doppler-free lines of molecular iodine [20] in a separate experiment [16]. The corrected wave number can be written in the form

$$\sigma_c = (1 + k_{\mathrm{eff}})\,\sigma_u, \tag{1}$$

where σ_c is the corrected wave number, σ_u is the uncorrected wave number and k_{eff} is the correction factor derived from the four ^{198}Hg internal standard lines [16]. For each spectrum the value of k_{eff} is taken to be the average of the values determined from each of the four Hg lines and its uncertainty is the standard deviation of those values.

In table 1 we present our measurements of wave numbers of Ar I atomic lines corrected according to equation (1). In the first and the second column we give the line number and the approximate wavelength in air ('line name') of each line, respectively. Columns 3 and 4 specify the lower and the upper

Table 1. Wave numbers of argon emission lines measured at pressures of 1333, 933, 400 and 33 Pa (10, 7, 3 and 0.25 Torr), and the wave numbers corresponding to zero argon pressure (0 Pa column). Uncertainties are given at a 95% level of confidence.

Line no.	Line name	Level		1333 Pa wave number (cm^{-1})	933 Pa wave number (cm^{-1})	400 Pa wave number (cm^{-1})	33 Pa wave number (cm^{-1})	0 Pa wave number (cm^{-1})
		Lower	Upper					
1	355.4 nm	$({}^2\mathrm{P}_{3/2})$ 4s$[3/2]_2$	$({}^2\mathrm{P}_{3/2})$ 6p$[3/2]_2$				28 126.8629(4)	
2	356.7 nm	$({}^2\mathrm{P}_{3/2})$ 4s$[3/2]_2$	$({}^2\mathrm{P}_{3/2})$ 6p$[5/2]_3$				28 021.6107(6)	
3	360.6 nm	$({}^2\mathrm{P}_{3/2})$ 4s$[3/2]_1$	$({}^2\mathrm{P}_{3/2})$ 6p$[1/2]_0$				27 719.6445(4)	
4	383.4 nm	$({}^2\mathrm{P}_{1/2})$ 4s$[1/2]_1$	$({}^2\mathrm{P}_{3/2})$ 6p$[1/2]_0$				26 070.4140(4)	
5	394.7 nm	$({}^2\mathrm{P}_{3/2})$ 4s$[3/2]_2$	$({}^2\mathrm{P}_{1/2})$ 5p$[3/2]_2$				25 325.2930(4)	
6	394.8 nm	$({}^2\mathrm{P}_{3/2})$ 4s$[3/2]_2$	$({}^2\mathrm{P}_{1/2})$ 5p$[1/2]_1$	25 315.8347(7)	25 315.8364(12)	25 315.8379(7)	25 315.8393(2)	25 315.8394(5)
7	404.4 nm	$({}^2\mathrm{P}_{3/2})$ 4s$[3/2]_1$	$({}^2\mathrm{P}_{1/2})$ 5p$[3/2]_2$	24 718.4500(6)	24 718.4514(9)	24 718.4547(5)	24 718.4559(2)	24 718.4561(5)
8	415.8 nm	$({}^2\mathrm{P}_{3/2})$ 4s$[3/2]_2$	$({}^2\mathrm{P}_{3/2})$ 5p$[3/2]_2$	24 039.8256(2)	24 039.8274(2)	24 039.8309(1)	24 039.8329(2)	24 039.8331(4)
9	416.4 nm	$({}^2\mathrm{P}_{3/2})$ 4s$[3/2]_2$	$({}^2\mathrm{P}_{3/2})$ 5p$[3/2]_1$	24 007.5637(7)	24 007.5629(12)	24 007.5650(6)	24 007.5680(2)	24 007.5680(6)
10	418.1 nm	$({}^2\mathrm{P}_{1/2})$ 4s$[1/2]_0$	$({}^2\mathrm{P}_{1/2})$ 5p$[1/2]_1$	23 905.9286(7)	23 905.9297(10)	23 905.9322(5)	23 905.9345(2)	23 905.9346(5)
11	419.0 nm	$({}^2\mathrm{P}_{3/2})$ 4s$[3/2]_2$	$({}^2\mathrm{P}_{1/2})$ 5p$[5/2]_2$	23 855.5612(5)	23 855.5640(7)	23 855.5653(4)	23 855.5674(2)	23 855.5675(6)
12	419.1 nm	$({}^2\mathrm{P}_{1/2})$ 4s$[1/2]_0$	$({}^2\mathrm{P}_{1/2})$ 5p$[3/2]_1$	23 853.7610(7)	23 853.7623(10)	23 853.7653(5)	23 853.7666(2)	23 853.7667(5)
13	419.8 nm	$({}^2\mathrm{P}_{3/2})$ 4s$[3/2]_1$	$({}^2\mathrm{P}_{3/2})$ 5p$[1/2]_0$	23 812.3533(4)	23 812.3550(4)	23 812.3583(2)	23 812.3605(2)	23 812.3607(4)
14	420.0 nm	$({}^2\mathrm{P}_{3/2})$ 4s$[3/2]_2$	$({}^2\mathrm{P}_{3/2})$ 5p$[5/2]_3$	23 798.9905(2)	23 798.9921(2)	23 798.9949(1)	23 798.9968(2)	23 798.9969(3)
15	425.1 nm	$({}^2\mathrm{P}_{3/2})$ 4s$[3/2]_2$	$({}^2\mathrm{P}_{3/2})$ 5p$[1/2]_1$	23 516.2260(20)	23 516.2291(24)		23 516.2357(4)	23 516.2360(6)
16	425.9 nm	$({}^2\mathrm{P}_{1/2})$ 4s$[1/2]_1$	$({}^2\mathrm{P}_{1/2})$ 5p$[1/2]_0$	23 471.0893(11)	23 471.0871(7)	23 471.0891(3)	23 471.0901(2)	23 471.0902(4)
17	426.6 nm	$({}^2\mathrm{P}_{3/2})$ 4s$[3/2]_1$	$({}^2\mathrm{P}_{3/2})$ 5p$[3/2]_2$	23 432.9883(5)	23 432.9907(6)	23 432.9940(4)	23 432.9955(2)	23 432.9958(4)
18	427.2 nm	$({}^2\mathrm{P}_{3/2})$ 4s$[3/2]_1$	$({}^2\mathrm{P}_{3/2})$ 5p$[3/2]_1$	23 400.7246(3)	23 400.7266(4)	23 400.7286(2)	23 400.7305(2)	23 400.7306(4)
19	430.0 nm	$({}^2\mathrm{P}_{3/2})$ 4s$[3/2]_1$	$({}^2\mathrm{P}_{3/2})$ 5p$[5/2]_2$	23 248.7237(4)	23 248.7253(6)	23 248.7279(3)	23 248.7300(2)	23 248.7301(5)
20	433.3 nm	$({}^2\mathrm{P}_{1/2})$ 4s$[1/2]_1$	$({}^2\mathrm{P}_{1/2})$ 5p$[3/2]_2$	23 069.2227(6)	23 069.2221(9)	23 069.2239(4)	23 069.2254(3)	23 069.2253(6)
21	433.5 nm	$({}^2\mathrm{P}_{1/2})$ 4s$[1/2]_1$	$({}^2\mathrm{P}_{1/2})$ 5p$[1/2]_1$	23 059.7680(15)	23 059.7692(26)	23 059.7723(12)	23 059.7711(3)	23 059.7712(6)
22	434.5 nm	$({}^2\mathrm{P}_{1/2})$ 4s$[1/2]_1$	$({}^2\mathrm{P}_{1/2})$ 5p$[3/2]_1$	23 007.5984(17)	23 007.6019(29)	23 007.6006(14)	23 007.6030(3)	23 007.6031(7)
23	451.0 nm	$({}^2\mathrm{P}_{1/2})$ 4s$[1/2]_1$	$({}^2\mathrm{P}_{3/2})$ 5p$[1/2]_0$	22 163.1264(12)	22 163.1258(16)	22 163.1283(9)	22 163.1300(3)	22 163.1301(5)
24	452.2 nm	$({}^2\mathrm{P}_{1/2})$ 4s$[1/2]_0$	$({}^2\mathrm{P}_{3/2})$ 5p$[1/2]_1$	22 106.3250(24)			22 106.3305(4)	22 106.3307(9)

levels involved in the transition[2]. Measured wave numbers for the four argon pressures are given in the next four columns. In the last column we give the wave numbers for the 19 strongest argon lines at zero pressure. The zero pressure wave numbers are determined as the intercept of the regression lines calculated through the wave numbers measured at all four pressures, as discussed below[3].

Each wave number in table 1 represents the average of four to eight individual measurements weighted by the inverse square of their uncertainties, 75% of the lines having eight measurements. The uncertainty of the average value is calculated as the quadrature sum of (a) the standard deviation of the weighted average, (b) the portion of the calibration uncertainty that is attributable to the uncertainty in the internal standard lines, and (c) a non-statistical relative uncertainty of 6.16×10^{-9} which represents the limiting accuracy of the multiplicative correction of the wave number scale for our FTS as determined in [16]. The uncertainties of strong lines with high signal-to-noise ratio (SNR) are dominated mostly by this last contribution, whereas the uncertainties of weak lines with low SNR are dominated mostly by statistical contributions. The quadrature sum of the three contributions constitutes the uncertainty in the wave number at the one standard deviation level. The uncertainties we report in table 1 have been expanded by a factor of 2 to provide a 95% confidence level.

In figure 1 we compare our measurements of the Ar I wave numbers with the most comprehensive sets of similar measurements published in the last four decades. In the first of these studies, published by Norlén [4] in 1973, 233 Ar I lines and 354 Ar II lines were observed in a water-cooled hollow cathode discharge run in pure argon at a pressure of 26.7 Pa (0.2 Torr). The argon was circulated through liquid nitrogen cooled traps during the observations. The spectral lines were measured using photographic Fabry–Pérot interferometry. ^{86}Kr I lines from a microwave-excited EDL served as standards. Figure 1(a) shows the differences between the results of Norlén and wave numbers calculated from our data for a pressure of 26.7 Pa. The differences are uniformly positive showing that Norlén's wave numbers are systematically smaller than ours by approximately 0.0015 cm^{-1}.

The second study was published by Li and Humphreys [3] in 1974. In this experiment 307 Ar I lines were excited in microwave-excited EDLs. The sealed lamps were filled with argon at a pressure of 400–665 Pa (3–5 Torr) [37]. Their design included an argon reservoir, in which there was no discharge to stabilize the pressure. The lamps were operated in a cryostat at the triple point of nitrogen (63.18 K). At this temperature argon is a solid with vapour pressure of approximately 1333 Pa (10 Torr). Since this vapour pressure is higher than the pressure at which the lamps were filled, the argon remains in the gas phase and the operating pressure is between 84 and

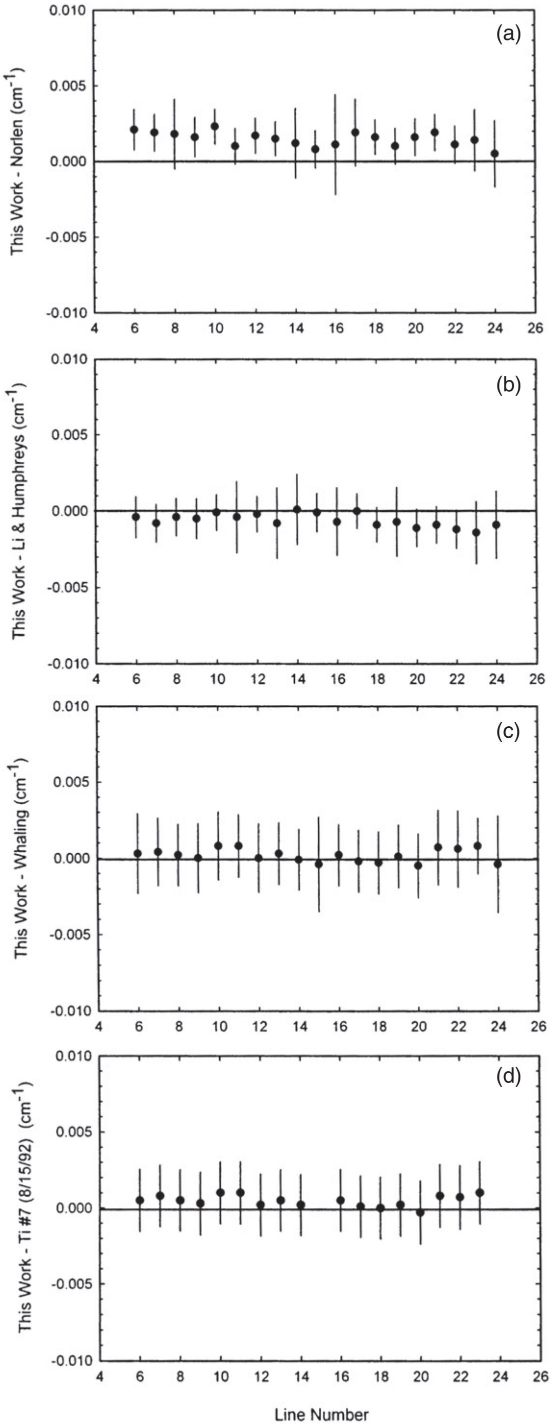

Figure 1. Comparison of wave numbers of 19 Ar I emission lines measured in this experiment with measurements of (a) Norlén [4], (b) Li and Humphreys [3], (c) Whaling *et al* [6], and (d) Kitt Peak spectrum Ti #7 (8/15/92) [21]. Line number corresponds to the row where the line appears in table 1. The error bars represent the uncertainties of the wave numbers measured in this work at a 95% level of confidence.

---

[2] The Racah notation for atomic levels is used. In common with all noble gases Ar I exhibits jK coupling. The states in Racah notation, based upon jK coupling, are labelled as $nl[K]_J$, where n and l are the principal and orbital angular momentum quantum numbers of the valence electron, and $\boldsymbol{K} = \boldsymbol{J}_c + \boldsymbol{l}$, where $\mathbf{J}_c$ is the angular momentum of the core. The manifold of the lowest ns states has four fine-structure states, $4s[1/2]_{0,1}$ and $4s[3/2]_{1,2}$. The 5p and 6p manifolds consist of ten states [26].

[3] The regression analysis was performed using the '*R*' statistical package. *R* is an open square integrated suite for data manipulation, calculation, and graphical display. Identification of this software is made to adequately specify our procedures. Such identification does not imply recommendation or endorsement by the National Institute of Standards and Technology, nor does it imply that the product identified is necessarily the best available for the purpose.

140 Pa (0.63 and 1.05 Torr). The spectra were measured using a temperature controlled evacuated Fabry-Pérot interferometer in conjunction with a 3.4 m Ebert plane-grating spectrograph. ^{86}Kr I lines from a microwave-excited EDL cooled to the triple point of nitrogen were used as standards. In figure 1(b) we present the differences between the results of Li and Humphrey and our wave numbers. For purposes of this comparison we have assumed an argon pressure of 84 Pa. The wave numbers of Li and Humphrey are systematically larger than ours by approximately 0.0009 cm^{-1}. The assumption of higher argon pressure would increase the discrepancy.

The most comprehensive line list for argon is given by Whaling *et al* [6] in a 2002 paper. In this work 928 Ar I lines were measured by analysing six high-resolution spectra of hollow cathode discharges in argon with a variety of cathode materials. All of the spectra were recorded on the 1 m vacuum FTS of the National Solar Observatory at the Kitt Peak National Observatory. According to the authors, the argon pressure varied from one spectrum to another between 270 Pa (2 Torr) and 530 Pa (4 Torr). A recent reanalysis of these data [21] revealed that the wave numbers published in [6] should be corrected by a constant multiplicative factor of 0.999 999 933. In addition, the three spectra that were used by Whaling *et al* in the wavelength region that can be compared with our measurements were recorded at argon pressures of 80 Pa (0.6 Torr) and 200 Pa (1.5 Torr). In figure 1(c) we present the differences between Whaling and our wave numbers (calculated as the average from our data for pressures of 80 Pa and 200 Pa). Whaling's wave numbers are slightly smaller than ours with an average deviation of 0.0002 cm^{-1}. In figure 1(d) we compare our results with measurements from the spectrum Ti #7 (8/15/92) that was recorded at an argon pressure of 82 Pa. This is one of the spectra used by Whaling *et al*. The interferogram was downloaded from the Kitt Peak archive, transformed, and measured in [21]. We show the comparison because the argon pressure is accurately known for this spectrum. The results are smaller than our current values with an average deviation of 0.0005 cm^{-1}. We conclude that, after making the correction suggested in [21], the results of Whaling *et al* show the best agreement with our measurements. However, the uncertainty of our data is smaller by an order of magnitude.

3.2. Pressure shifts

In figure 2 we present results of our measurements of the pressure dependence for each line obtained by making a linear least squares fit to the data (see footnote 3). All individual measurements were included in the fit with weights inversely proportional to the square of their uncertainties. In addition to the zero-pressure wave number, this regression analysis delivers the pressure shift rate (PSR) for each line, the relative error of the PSR, and the upper and the lower confidence band limits for wave numbers calculated from the fitted zero pressure wave number and PSR (dashed curves in figure 2). Most of the lines presented in figure 2 show a clear linear dependence of the shift on the pressure, with a small scatter of data points. These lines have a high signal-to-noise ratio (SNR) in the observed spectra. A few of the weaker lines show a large scatter in the measurements, especially at higher argon pressures where their SNR is lowest. This is reflected in the width of the 95% confidence interval for these lines.

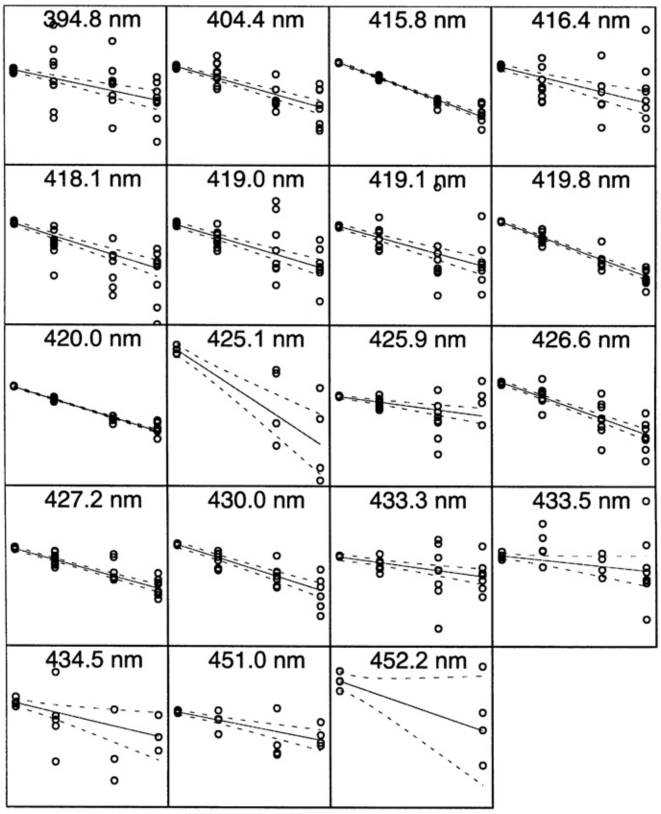

Figure 2. Dependence of wave numbers of 19 Ar I lines on argon pressure. For each subplot pressure is given on the horizontal axis and the wave number on the vertical axis. Data points are shown at argon pressures of 33, 400, 933 and 1333 Pa increasing to the right. For all lines the wave number data are mean-centred and the full height of the vertical axis represents 0.023 cm^{-1}. Broken curves correspond to the upper and the lower 95% confidence limits for the fit to the wave numbers.

3.2.1. Recapitulation of the line shift and broadening theory.

Since pressure shift (and broadening) of spectral lines takes place due to atomic interactions, in general one can learn about underlying atom–atom interactions by analysing the pressure broadening and shift data. The red shift observed for all lines with increasing pressure (figure 2) indicates that the essential contribution to the shift comes from the attractive long-range tail of the argon–argon interatomic potential. In order to relate the line-shifts determined in our experiment to the details of the atom–atom interactions, we will briefly review the theory of line-shift and broadening.

Theories of line-shift and broadening are usually divided into two limiting cases: the low-pressure, impact collision limit, and the high-pressure, statistical limit [22]. In the low-pressure limit the time between collisions is long compared to the duration of collisions, and three-body (and higher order) collisions may be neglected. Thus, interactions affecting the line-shift and the line shape can be understood through studies of binary atomic collisions. The collision is modelled as a scattering event, which depends on the relative motion between the emitting and the perturbing atom, as well as on the atom–perturber interaction potential. Our experiments were performed in the low-pressure regime, where the impact theory of line-shift and broadening is valid. The fact that the shifts shown in figure 2 all vary linearly with the perturber pressure is a clear indication that the impact approximation is valid over the range of argon pressures involved, since perturbations due to collisions are expected to be linearly proportional to the density of perturbing atoms in this approximation. The magnitude of the shift, however, depends on the strength and the type of the atomic interaction as well as on the number of collisions.

In the case of self-broadening at low pressure, the Lindholm–Foley impact theory [23, 24] predicts a Lorentzian line-shape

$$L(\nu,\gamma,\beta) = (\gamma/\pi)/[(\nu-\nu_0-\beta)^2+\gamma^2], \tag{2}$$

where ν_0 is the centre frequency of the unshifted line, γ is the collision half-width at half-maximum (HWHM), and β is the collision induced line-shift. The quantities β and γ are given as

$$\beta = v_m\sigma_I(v_m)N, \tag{3}$$

$$\gamma = v_m\sigma_R(v_m)N, \tag{4}$$

where σ_I and σ_R are the shift and broadening cross sections and N is the density of perturbing atoms. Here v_m denotes the mean relative velocity $v_m = (8k_BT/\pi\mu)^{1/2}$, where k_B is the Boltzmann constant, T the absolute temperature and μ the reduced mass of the colliding atoms. The ratios β/N and γ/N are known as the line-shift and broadening constants. Note that line-shift and broadening constants are most frequently given in the units of cm^{-1}/(atoms cm^{-3}) or s^{-1}/(atoms cm^{-3}) [25]. If the line width and the line-shift are expressed in cm^{-1}, the designation is usually $\Delta\nu_{1/2}$ for the full width at half maximum (FWHM), and $\Delta\nu_0$ for the line-shift. If expressed in s^{-1} the common designation is γ (or w) for the line half-width at half maximum (HWHM) and β (or d) for the line-shift. The two different notations are related as [25]

$$\beta/N = (2\pi c)(\Delta\nu_0/N), \tag{5}$$

and

$$2\gamma/N = (2\pi c)(\Delta\nu_{1/2}/N). \tag{6}$$

However, the pressure shift and broadening constants depend not only on the nature of the atomic interactions, but also on the gas temperature and atomic masses. The presentation of the pressure broadening and shift data only in the form of pressure shift and broadening constants obscures their temperature and mass dependence. Consequently, it is useful to present the same data as shift and broadening cross sections, σ_I and σ_R, derived from the pressure shift and broadening constants via the expressions (3) and (4)

$$\sigma_I = (\beta/N)/v_m \tag{7}$$

and

$$\sigma_R = (\gamma/N)/v_m. \tag{8}$$

Providing the atomic interactions are known, the pressure shift and broadening cross sections can be calculated as [23]

$$\sigma_I(v_m) = 2\pi\int_o^\infty \sin\eta(\rho, v_m)\rho\,\mathrm{d}\rho \tag{9}$$

and

$$\sigma_R(v_m) = 2\pi\int_o^\infty \{1-\cos\eta(\rho, v_m)\}\rho\,\mathrm{d}\rho. \tag{10}$$

These equations relate the shift and broadening parameters to the interatomic potentials $V(R)$ via the quantity $\eta(\rho, v_m)$, the total phase change produced in a collision with an impact parameter ρ (the distance of closest approach of the collision particles) and a mean relative velocity v_m. The total phase change produced in a collision with an impact parameter ρ is given by

$$\eta(\rho, v_m) = \int_{-\infty}^{\infty} \{\Delta V[R(t)]/\hbar\}\,\mathrm{d}t. \tag{11}$$

Here the quantity $\Delta V(R)$, given as

$$\Delta V(R) = V_u(R) - V_l(R) \tag{12}$$

is known as the difference interaction potential. $V_u(R)$ and $V_l(R)$ are the interaction potentials for the upper and the lower state of a transition in the argon atom, and $R(t,\rho) = [\rho^2 + {v_m}^2 t^2]^{1/2}$ is the interatomic separation in the straight path approximation with t the time relative to the time of closest approach.

The total phase shift $\eta(\rho, v_m)$, and consequently all pressure shift (and broadening) data, depend on the nature of the interaction of the emitting and the perturber atoms. Collisions involving large impact parameters produce small phase changes of less than 1 rad, but are effective in shifting the mean wavelength of the spectral line. The effects of weak but frequent distant collisions are cumulative, so that small but numerous perturbations lead to a measurable shift of the line. On the other hand, strong collisions with small impact parameters produce larger changes in the phase of the radiation and are effective in producing line broadening. Consequently, the shift rates are much more sensitive to the real form of the difference potential than the broadening rates since they depend not only on the strength but also on the shape of the outer part of the interatomic potential.

3.2.2. Interaction potential. The Lennard-Jones potential is often chosen as a model atomic interaction potential [23, 24]. This potential is given by $V(R) = C_{12}R^{-12} - C_6R^{-6}$ ($C_6 > 0$, $C_{12} > 0$). Generally, it is a relatively realistic model for atomic interactions, taking into account not only the long-range attraction of van der Waals type, but also a strong repulsion at smaller distances [26].

The level van der Waals constant, C_6, is often calculated according to the formula [27]

$$C_6 = \alpha_0\, e^2\langle r_k^2\rangle, \tag{13}$$

where α_0 is the static polarizability of the perturber atom, e is the electron charge, and $\langle r_k^2\rangle$ is the quantum mechanical expectation value of the mean square radius of the valence electron in state $|k\rangle$ of the radiating atom. In the case of a hydrogenic atom the mean square radius can be calculated

Table 2. Calculated mean square radii of the valence electron in excited states of Ar I and corresponding C_6 constants. The data are given in atomic units (au). The ionization potential of argon is 127 109.842 cm^{-1} [31]. The absolute uncertainties in the calculated values are estimated to be about 30%. We retain more significant figures in the table to display the differences between values for levels with the same J_c and l. For the $(^2P_{1/2})5p[1/2]_0$ level we were not able to obtain convergence in the HF approximation. Note the difference between CA and HF calculations in the case of the highest argon levels.

Level	Energy (cm^{-1})	$\langle r^2\rangle$ (au)[a]	C_6 (au)[b]	$\langle r^2\rangle$ (au)[a]	C_6 (au)[b]
		Coulomb approximation (CA)		Hartree–Fock approximation (HF)	
$(^2P_{3/2})$ 4s$[3/2]_2$	93 143.760	27.71	−304.8	30.22	−332.4
$(^2P_{3/2})$ 4s$[3/2]_1$	93 750.598	28.70	−315.7	30.75	−338.2
$(^2P_{1/2})$ 4s$[1/2]_0$	94 553.665	30.09	−331.0	30.22	−332.4
$(^2P_{1/2})$ 4s$[1/2]_1$	95 399.828	31.67	−348.4	32.31	−355.4
$(^2P_{3/2})$ 5p$[1/2]_1$	116 659.993	249.43	−2743.7	251.80	−2769.7
$(^2P_{3/2})$ 5p$[5/2]_3$	116 942.754	264.25	−2906.7	267.80	−2945.7
$(^2P_{3/2})$ 5p$[5/2]_2$	116 999.326	267.37	−2941.0	272.00	−2991.9
$(^2P_{3/2})$ 5p$[3/2]_1$	117 151.326	276.01	−3036.1	279.70	−3076.6
$(^2P_{3/2})$ 5p$[3/2]_2$	117 183.590	277.90	−3056.9	281.20	−3093.1
$(^2P_{3/2})$ 5p$[1/2]_0$	117 562.955	301.57	−3317.2	290.10	−3191.0
$(^2P_{1/2})$ 5p$[3/2]_1$	118 407.430	365.99	−4025.9	271.60	−2987.5
$(^2P_{1/2})$ 5p$[1/2]_1$	118 459.598	370.61	−4076.7	277.20	−3049.1
$(^2P_{1/2})$ 5p$[3/2]_2$	118 469.051	371.46	−4086.0	274.20	−3016.1
$(^2P_{1/2})$ 5p$[1/2]_0$	118 870.917	410.20	−4512.2	–	–

[a] 1 au = $a_0{}^2$ where a_0 denote the Bohr radius.

[b] 1 au = $a_0{}^5e^2$, where e denotes the electron charge.

exactly using the Coulomb approximation, and is given by [27, 28]

$$\left\langle r_k^2\right\rangle = 0.5(a_0)^2(n_k^*)^2[5(n_k^*)^2 + 1 - 3l(l+1)], \qquad (14)$$

where a_0 is the Bohr radius, $n_k{}^*$ is the effective principal quantum number of the state $|k\rangle$, and l is the orbital angular momentum quantum number.

The accuracy of the van der Waals constants depends on the magnitude of the mean square radius of the valence electron and on the static polarizability of argon atoms. Since the static polarizability of argon atoms is known rather accurately ($\alpha_0 = 11\ a_0{}^3 \pm 10\%$, see [29] and references therein), the accuracy of the calculated van der Waals constant for a given level depends primarily on an accurate knowledge of the mean square radius of the valence electron. Equation (14), is widely used in calculations of the mean square radius of the valence electron, implicitly assuming that the Coulomb approximation and hydrogenic wavefunctions can be used to describe valence states of complex atoms. Since it can be calculated exactly only in the case of a hydrogenic atom, a calculation of this kind is of limited value for complex atoms, and the uncertainty is expected to be large for heavy elements and for atoms with more than one valence electron [24, 27, 28]. Therefore, equation (14) may be too crude an approximation in the case of argon. To check this possibility, we compared the $\left\langle r_k^2\right\rangle$ calculated in the Coulomb approximation (CA) with values derived from radial wavefunctions calculated using the Cowan atomic structure program RCN [30]. The radial functions were calculated in the single configuration LS term dependent Hartree–Fock (HF) approximation. Relativistic and correlation corrections were included in the calculations. Empirical intermediate coupling eigenvectors for the levels of the 3p^{5}4s and 3p^{5}5p configurations were determined using the Cowan program RCE, and these eigenvectors were used to produce appropriate linear combinations of the LS term dependent radial wavefunctions for each state [30].

The results are given in table 2. The HF and CA values of $\left\langle r_k^2\right\rangle$ agree within 5% in the case of lower levels, but more significant differences exist in the case of the highest lying levels, where the CA and HF calculations disagree by 30%. We have used the values for $\left\langle r_k^2\right\rangle$ calculated in the HF approximation for calculations of the C_6 and pressure shift constants.

The appropriate way to calculate the level C_{12} constants in the case of interaction of similar or dissimilar noble gas atoms is, according to [23]

$$C_{12} = qR^{12}, \qquad (15)$$

where q is a constant and $R = R^* + R_0$. R^* and R_0 represent the radii of the excited atom and the perturber atom (in the ground state) where the radial charge density has the appropriate value. Hindmarsh found that, for either Coulomb or Hartree–Fock wavefunctions, defining R^* and R_0 to be the radii at which the radial charge density is 0.012 atomic units, and taking the value for q to be $(0.9 \pm 0.3) \times 10^{-23}$ J gave best agreement with experimental results [23]. The radii R^* and R_0 have also been calculated using intermediate coupling radial wavefunctions constructed as described above.

For the Lindholm–Foley theory of impact line broadening, assuming that the atoms move in classical straight paths, one obtains the following expressions for the total phase shift as well as for the line-shift and broadening constants [23]:

$$\eta(\rho, v_m) = (63\pi/256)(\Delta C_{12}/\hbar v_m)\rho^{-11} - (3\pi/8)(\Delta C_6/\hbar v_m)\rho^{-5}, \qquad (16)$$

$$\beta/N = (2\pi)(3\pi/8)^{2/5}S(\alpha)v_m^{3/5}[\Delta C_6/\hbar]^{2/5}, \qquad (17)$$

$$2\gamma/N = 4(\beta/N)[B(\alpha)/S(\alpha)], \qquad (18)$$

where

$$\alpha = (63\pi/256)(8/3\pi)^{11/5}(\hbar)^{6/5}v_m^{6/5}\Delta C_{12}|\Delta C_6|^{-11/5}. \qquad (19)$$

The dimensionless functions $S(\alpha)$ and $B(\alpha)$ have been tabulated by Hindmarsh *et al* [32]. The ΔC_6 and ΔC_{12} constants appearing in the equations (16)–(17) are known as effective C_6 and C_{12} constants, where $\Delta C_n = C_n^{\mathrm{up}} - C_n^{\mathrm{low}}$, represents the difference of the level constants for the upper and the lower levels of the transition. In the limit of a pure van der Waals interaction (i.e. if $C_{12} \to 0$ and $\Delta C_{12} \to 0$) equations (18) and (19) smoothly reduce to the well-known relations $\beta/N = -2.96\, v_m^{3/5}\, [(\Delta C_6/\hbar]^{2/5}$ and $2\gamma/N = -2.76\, \beta/N$.

The ΔC_6 constant is an effective van der Waals constant, corresponding to the long-range part of the Lennard-Jones difference interaction potential of the type $\Delta V(R) = \Delta C_{12} R^{-12} - \Delta C_6 R^{-6}$. Since the $\langle r_k^2 \rangle$ of the valence electron is at least one order of magnitude larger in the upper level than in the lower level, the effective van der Waals constants are heavily dominated by the upper state of the transition. The ΔC_{12} constant is also an effective constant, corresponding to the short-range part of the Lennard-Jones difference interaction potential. Note that ΔC_{12} is also heavily dominated by the upper state of the transition, since the C_{12} constant for the upper level is at least one to two orders of magnitude larger than the C_{12} constant for the lower level.

The assumed shape of the path travelled by the colliding atoms can influence the calculations of the shift and broadening parameters. Following [23] a simple qualitative test can be made to estimate the applicability of the straight-path approximation. The trajectory will be significantly curved if the impulse of the force exerted between the colliding atoms becomes of the order of the momentum of either of them. The relevant ratio is therefore

$$p = \left[\int F\,\mathrm{d}t\right] \Big/ \mu v \approx (6/\mu)(\hbar^6/v^4\, C_6)^{1/5}. \tag{20}$$

If $p \approx 1$ the trajectory is significantly curved, but if $p \ll 1$ it is practically unaltered by the interatomic forces and the approximation of a straight-path is justified. Since in our experiment $p \approx 0.04$ we can use, with confidence, the impact approximation assuming a straight-path trajectory of the colliding atoms. However, it should be noted that straight-line trajectories are apparently better suited for computations of line-width and are less satisfactory for line-shift [33].

In table 3, we summarize our measurements and calculations of pressure shift data for the 19 strongest Ar I atomic lines. The lines are presented in four groups according to the lower level of the transition, since the shifts of the lines sharing the same lower level show a similar behaviour. The first group comprises the lines terminating on the $4s[3/2]_2$ level, the second on $4s[3/2]_1$, the third on $4s[1/2]_0$ and fourth group on the $4s[1/2]_1$ level. Levels with $J = 0$ and 2 are metastable levels, whereas levels with $J = 1$ are resonance levels.

In the first column of table 3, each line is identified by its approximate air wavelength in nm. Columns 2 and 3 specify the lower and the upper levels involved in the transition. Measured pressure shift rates are given in fourth column. The pressure shift constants (determined from the pressure shift rates) are given in the next four columns. The measured pressure shift constants are compared with the pressure shift constants calculated using the Lennard-Jones (and pure van der Waals) interaction potentials, with HF radial wavefunctions. In the last column we give the pressure shift cross sections determined from the pressure shift constants. The reported uncertainties are expanded to provide a 95% confidence level.

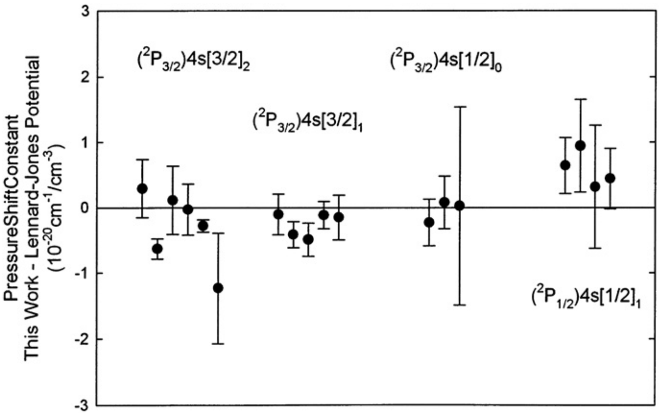

Figure 3. Comparison of the measured argon pressure shift constants for 18 Ar I lines to calculated constants based on a Lennard-Jones interaction potential. The lines in this figure are arranged in four groups according to the lower level of the transition. The error bars of the measured pressure shift constants are given at a 95% level of confidence.

Based on the comparison between CA and HF presented in table 2, one can expect that the calculation of $\langle r_k^2 \rangle$ has an overall accuracy of about ± 30%. Since the static polarizability of argon atoms is known with a relative uncertainty of about ± 10% one can expect that the calculated C_6 constants may have an overall accuracy of about ± 30%–± 40%. Note that the intrinsic accuracy of C_{12} constants is about 30%, too. Attributing a 30%–40% overall uncertainty to the calculations, the absolute agreement between theory and experiment can be regarded as satisfactory.

We note that, although the line-shift constants calculated in the HF approximation do not differ significantly from the line-shift constants calculated in the CA approximation, it appears that the Lennard-Jones interaction picture with HF calculated C_6 constants provides a marginally better description of the Ar*–Ar interatomic potentials.

To our knowledge, there are only two experiments in which pressure broadening and shift of lines belonging to the $3p^55p$–$3p^54s$ transition array were studied [13, 14]. In column 6 the pressure shift constants measured in our experiment are compared to the pressure shift constants of the line at 415.8 nm measured by Aeschliman *et al* [13] and of the line at 430.0 nm measured by Bielski *et al* [14]. The results are in satisfactory agreement for the 430.0 nm line [14], but in strong disagreement for the 415.8 nm line measured in [13].

The measured and the calculated pressure shift constants are graphically presented in figure 3, in order to facilitate the comparison between theory and experiment. The points represent the differences between measured and calculated pressure shift constants. The error bars represent the experimental uncertainties from table 3. One can observe that the shifts of the lines sharing the same lower level have a similar behaviour. The transitions with the lower levels $(^2P_{3/2})4s[3/2]_2$ and $(^2P_{3/2})4s[1/2]_0$, generally agree well

Table 3. Argon pressure shift rates (PSR), shift constants ($\Delta\nu_0/N$) and shift cross sections (σ_I) measured and calculated in this experiment compared to the measurements reported by Aeschliman *et al* [13] and Bielski *et al* [14]. The lines in this table are presented in four groups according to the lower level of the transition. Uncertainties are given at a 95% level of confidence.

	Level		Pressure shift rates,	Pressure shift constants, $\Delta\nu_0/N$ ($10^{-20}\mathrm{cm}^{-1}/\mathrm{cm}^{-3}$)				Pressure shift cross sections, σ_I (10^{-14} cm^{-2})	
Line name	Lower	Upper	PSR ($10^{-6}\mathrm{cm}^{-1}/\mathrm{Pa}$) Experiment (this work)	Experiment (this work)	Experiment (other data)	Calc, vdW (this work)	Calc, LJ (this work)	Experiment (this work)	Experiment (other data)
394.8 nm	$({}^2\mathrm{P}_{3/2})$ 4s$[3/2]_2$	$({}^2\mathrm{P}_{1/2})$ 5p$[1/2]_1$	−3.49 ± 1.15	−1.35 ± 0.45		−1.57	−1.65	4.68 ± 1.54	
415.8 nm	$({}^2\mathrm{P}_{3/2})$ 4s$[3/2]_2$	$({}^2\mathrm{P}_{3/2})$ 5p$[3/2]_2$	−5.72 ± 0.38	−2.22 ± 0.15	−0.34 ± 0.02[a]	−1.58	−1.59	7.67 ± 0.50	1.03 ± 0.04 [a]
416.4 nm	$({}^2\mathrm{P}_{3/2})$ 4s$[3/2]_2$	$({}^2\mathrm{P}_{3/2})$ 6p$[3/2]_1$	−3.96 ± 1.36	−1.54 ± 0.53		−1.57	−1.65	5.31 ± 1.83	
419.0 nm	$({}^2\mathrm{P}_{3/2})$ 4s$[3/2]_2$	$({}^2\mathrm{P}_{1/2})$ 5p$[5/2]_2$	−4.62 ± 1.00	−1.79 ± 0.39		−1.55	−1.76	6.19 ± 1.33	
420.0 nm	$({}^2\mathrm{P}_{3/2})$ 4s$[3/2]_2$	$({}^2\mathrm{P}_{3/2})$ 5p$[5/2]_3$	−4.91 ± 0.25	−1.91 ± 0.10		−1.54	−1.63	6.58 ± 0.34	
425.1 nm	$({}^2\mathrm{P}_{3/2})$ 4s$[3/2]_2$	$({}^2\mathrm{P}_{3/2})$ 5p$[1/2]_1$	−7.48 ± 2.20	−2.90 ± 0.85		−1.50	−1.67	10.02 ± 2.95	
404.4 nm	$({}^2\mathrm{P}_{3/2})$ 4s$[3/2]_1$	$({}^2\mathrm{P}_{1/2})$ 5p$[3/2]_2$	−4.49 ± 0.82	−1.74 ± 0.32		−1.56	−1.64	6.02 ± 1.10	
419.8 nm	$({}^2\mathrm{P}_{3/2})$ 4s$[3/2]_1$	$({}^2\mathrm{P}_{3/2})$ 5p$[1/2]_0$	−5.70 ± 0.49	−2.21 ± 0.19		−1.60	−1.80	7.64 ± 0.65	
426.6 nm	$({}^2\mathrm{P}_{3/2})$ 4s$[3/2]_1$	$({}^2\mathrm{P}_{3/2})$ 5p$[3/2]_2$	−5.44 ± 0.66	−2.11 ± 0.25		−1.58	−1.62	7.29 ± 0.88	
427.2 nm	$({}^2\mathrm{P}_{3/2})$ 4s$[3/2]_1$	$({}^2\mathrm{P}_{3/2})$ 6p$[3/2]_1$	−4.49 ± 0.53	−1.74 ± 0.21		−1.57	−1.62	6.02 ± 0.72	
430.0 nm	$({}^2\mathrm{P}_{3/2})$ 4s$[3/2]_1$	$({}^2\mathrm{P}_{3/2})$ 5p$[5/2]_2$	−4.93 ± 0.89	−1.91 ± 0.34	−2.22 ± 0.32[b]	−1.55	−1.76	6.61 ± 1.19	7.30 ± 1.05 [b]
418.1 nm	$({}^2\mathrm{P}_{1/2})$ 4s$[1/2]_0$	$({}^2\mathrm{P}_{1/2})$ 5p$[1/2]_1$	−4.84 ± 0.94	−1.88 ± 0.37		−1.57	−1.65	6.49 ± 1.26	
419.1 nm	$({}^2\mathrm{P}_{1/2})$ 4s$[1/2]_0$	$({}^2\mathrm{P}_{1/2})$ 5p$[3/2]_1$	−4.34 ± 1.05	−1.68 ± 0.41		−1.55	−1.76	5.82 ± 1.41	
452.2 nm	$({}^2\mathrm{P}_{1/2})$ 4s$[1/2]_0$	$({}^2\mathrm{P}_{3/2})$ 5p$[1/2]_1$	−4.24 ± 3.90	−1.65 ± 1.51		−1.50	−1.67	5.68 ± 5.23	
425.9 nm	$({}^2\mathrm{P}_{1/2})$ 4s$[1/2]_1$	$({}^2\mathrm{P}_{1/2})$ 5p$[1/2]_0$	−2.33 ± 1.01	−0.90 ± 0.39		–	–	3.12 ± 1.36	
433.3 nm	$({}^2\mathrm{P}_{1/2})$ 4s$[1/2]_1$	$({}^2\mathrm{P}_{1/2})$ 5p$[3/2]_2$	−2.41 ± 1.11	−0.94 ± 0.43		−1.55	−1.58	3.23 ± 1.49	
433.5 nm	$({}^2\mathrm{P}_{1/2})$ 4s$[1/2]_1$	$({}^2\mathrm{P}_{1/2})$ 5p$[1/2]_1$	−1.85 ± 1.83	−0.72 ± 0.71		−1.56	−1.66	2.48 ± 2.45	
434.5 nm	$({}^2\mathrm{P}_{1/2})$ 4s$[1/2]_1$	$({}^2\mathrm{P}_{1/2})$ 5p$[3/2]_1$	−3.52 ± 2.42	−1.37 ± 0.94		−1.55	−1.68	4.72 ± 3.24	
451.0 nm	$({}^2\mathrm{P}_{1/2})$ 4s$[1/2]_1$	$({}^2\mathrm{P}_{3/2})$ 5p$[1/2]_0$	−3.22 ± 1.20	−1.25 ± 0.46		−1.59	−1.69	4.32 ± 1.60	

[a] Aeschliman *et al* [13].

[b] Bielski *et al* [14].

with the calculations based on the Lennard-Jones interaction potentials. Only three of the nine lines disagree outside the 95% confidence interval of the experimental data. On the other hand, transitions with the $(^2P_{3/2})4s[3/2]_1$ lower level show measured shifts slightly larger than the calculated ones, while transitions with the $(^2P_{3/2})4s[1/2]_1$ lower level show noticeably and systematically smaller measured shifts than calculated. Note that, unlike the $(^2P_{3/2})4s[3/2]_2$ and $(^2P_{3/2})4s[1/2]_0$ levels which are metastable and semi-metastable, the $(^2P_{3/2})4s[3/2]_1$ level is characterized by a weak, and the $(^2P_{3/2})4s[1/2]_1$ level by a strong resonance interaction. This means that, in the case of these two resonance levels, their level interaction potentials in the long range comprise not only one (the van der Waals) but two simultaneously acting interactions—the van der Waals and the resonance interaction.

The competition of two long-range interactions and its influence on the width and shift of atomic lines, is taken into account in the paper of Lewis [34]. Although his theory does not include the case when the short-range interactions are present simultaneously with the long-range ones, it can provide useful guidance in interpretation of our data. Since our calculations clearly show the dominant role of the van der Waals interaction in the shift data (see table 3), this approach is even more justified.

Lewis's theory predicts a reduction of the inherent (i.e. van der Waals) line-shift for lines perturbed simultaneously by van der Waals and resonant interactions. He defines the parameter $a = [2\gamma(3)/N]/[2\gamma(6)/N]$, measuring the relative strength of the resonance and van der Waals interactions. The terms $2\gamma(3)/N$ and $2\gamma(6)/N$ are the theoretical broadening coefficients for the resonance and van der Waals interactions, respectively. If $a < 1$, the broadening and shift should be weakly perturbed by the resonance interaction. If $a > 2$, the broadening is heavily dominated by resonance interaction, and the inherent (van der Waals) line-shift should be partially (50% or more) suppressed by the resonance interaction (see [34], figures 1 and 2).

Assuming oscillator strengths of 0.2214(68) for the strong $3p^6\,{}^1S_0$–$3p^5(^3P_{1/2})4s[1/2]_1$ transition, and 0.0580(17) for the weaker $3p^6\,{}^1S_0$–$3p^5(^3P_{3/2})4s[3/2]_1$ transition [35], we obtain $a \approx 0.7$ for the group of lines terminating on the $4s[3/2]_1$ resonance level and $a \approx 2.45$ for the group of lines terminating on the $4s[1/2]_1$ resonance level[4]. From calculated values of a one can read in figure 2 of [34] the corresponding predicted ratio of measured to inherent line-shift. For the group of lines terminating on the $4s[3/2]_1$ level ($a \approx 0.7$) this ratio is about 0.92, and for the group of lines terminating on the $4s[1/2]_1$ level ($a \approx 2.45$) it is about 0.3. In the case of lines terminating on the metastable levels $4s[3/2]_2$ and $4s[1/2]_0$, Lewis's theory predicts an essentially unperturbed van der Waals shift.

A closer inspection of our table 3 and figure 3 shows, indeed, that all lines terminating on the metastable levels or on the $4s[3/2]_1$ resonance level show similar, predominantly van der Waals behaviour, whereas the group of lines terminating on the $4s[1/2]_1$ resonance level clearly experiences a relatively strong reduction of inherent shifts. This reduction is not as strong as predicted by Lewis's theory (Lewis's predicted ratio of measured to inherent line-shift is about 0.3, whereas our experiment gives an average ratio about 0.6), but this can be expected in view of Lewis's own reservations about his shift calculations and the uncertainties in the calculation of parameter a [34].

In addition to the Lennard-Jones and van der Waals interaction potentials, we calculated the line-shifts using a more sophisticated representation of the Ar*–Ar interatomic potentials, a three-parameter potential of the type $V(R) = C_{12}R^{-12} - C_8R^{-8} - C_6R^{-6}$ ($C_6 > 0$, $C_8 > 0$, $C_{12} > 0$) [22]. Overall agreement with experiment is not as good as for the Lennard-Jones potential, and we have chosen not to present the details in this paper.

Our calculations confirm that, unlike the line-widths, the pressure shifts are very sensitive to the form of the potential defined by the C_n constants, and provide a critical test of the shape of the interatomic interactions. At larger effective quantum numbers n*, which are the case in our experiment, the atomic collisions cease to be dominated by long-range interactions, and the repulsive, short range interactions start to play an important role, since repulsive 'exchange' forces extend to progressively larger interatomic distances. It is very likely that a simple and convenient C_{12}/R^{12} form of the short-range potential is not good enough to represent its complexity. Furthermore, whereas the line-width is a sum of all positive terms, the line-shift involves both positive and negative contributions, and the resulting magnitude and sign of the shift are critically dependent on the interplay of the positive and negative contributions. They are, in turn, entirely dependent on the shape of the atomic interaction potentials. Last but not least, nonadiabatic processes will also be more important at larger n^* because of the density of nearby states (see e.g. calculations and pictures of potential energy curves for noble gas diatomic molecules in [36]). We believe that the remaining discrepancy between experiment and theory could be attributed mostly to the form of the interaction potentials.

4. Conclusions

We measured wave numbers and pressure-induced line-shifts of argon emission lines by using Fourier transform spectroscopy. The measurements were made using electrodeless lamps containing argon at four different pressures. Accurate calibration of the FTS wave number scale, obtained using the four most prominent ^{198}Hg emission lines, enabled determination of wave numbers of the UV/blue argon emission lines with high accuracy.

The measured pressure-induced shifts of the argon emission lines are in reasonable agreement with the theoretical predictions. The measurements and calculations suggest that the interaction of excited argon atoms with ground state argon atoms can be described with sufficient accuracy by an interaction potential of the Lennard–Jones type. A more accurate calculation of the line-shifts would require a more sophisticated theoretical approach for calculation of atomic

---

[4] The $4s[3/2]_1$ and $4s[1/2]_1$ levels correspond respectively to the levels designated $4s\,{}^3P_1$ and $4s\,{}^1P_1$ in the LS coupling notation.

interaction potentials of Ar*–Ar pairs, since line-shifts are particularly sensitive to the accuracy of the interatomic potentials.

Acknowledgment

Damir Veza gratefully acknowledges the hospitality of the NIST Atomic Spectroscopy Group.

References

[1] Burns K and Adams K B 1953 *J. Opt. Soc. Am.* **43** 1020
[2] Littlefield T A and Turnbull D T 1953 *Proc. R. Soc. London* **218** 577
[3] Li H H and Humphreys C J 1974 *J. Opt. Soc. Am.* **64** 1072
[4] Norlén G 1973 *Phys. Scr.* **8** 249
[5] Whaling W, Anderson W H C, Carle M T, Brault J W and Zarem H A 1995 *J. Quant. Spectrosc. Radiat. Transfer* **53** 1–22
[6] Whaling W, Anderson W H C, Carle M T, Brault J W and Zarem H A 2002 *J. Res. Natl Inst. Stand. Technol.* **107** 149
[7] Commission 14 General Assembly IAU 1957 *Trans. Int. Astron. Union* **IX** 201
[8] Commission 14 General Assembly IAU 1966 *Trans. Int. Astron. Union* **XIIB** 173
[9] Humphreys C J and Paul E Jr 1962 *J. Opt. Soc. Am.* **52** 591
[10] Murphy M T, Tzanavaris P, Webb J K and Lovis C 2007 *Mon. Not. R. Astron. Soc.* **378** 221
[11] Salit M L, Travis J C and Winchester M R 1996 *Appl. Opt.* **35** 2960
[12] Bengtson A, Eklund A and Praessler F 1996 *Fresenius J. Anal. Chem.* **355** 836
[13] Aeschliman D P, Hill R A and Evans D L 1976 *Phys. Rev.* A **14** 1421
[14] Bielski A, Pospieszny J, Szudy J, Trawinski R S and Wolnikovski J 1990 *J. Phys. B: At. Mol. Opt. Phys.* **23** 2003
[15] Veza D, Salit M L, Sansonetti C J and Travis J C 2005 *J. Phys. B: At. Mol. Opt. Phys.* **38** 3739
[16] Salit M L, Sansonetti C J, Veza D and Travis J C 2004 *J. Opt. Soc. Am.* B **21** 1543
[17] Fehsenfeld F C, Evenson K M and Broida H P 1963 *Rev. Sci. Instrum.* **36** 294
[18] Honig R E and Kramer D A 1969 *RCA Rev.* **30** 285
[19] Thorne A P, Harris C J, Wynne-Jones I, Learner R C M and Cox G 1987 *J. Phys. E: Sci. Instrum.* **20** 54
[20] Sansonetti C J 1997 *J. Opt. Soc. Am.* B **14** 1913
[21] Sansonetti C J 2007 *J. Res. Natl Inst. Stand. Technol.* **112** 297
[22] Allard N and Kielkopf J 1982 *Rev. Mod. Phys.* **54** 1103
[23] Hindmarsh W R and Farr J M 1972 *Prog. Quantum Electron.* **2** 141
[24] Schuller F and Behmenburg W 1974 *Phys. Rep.* **12** 273
[25] Lewis E L 1980 *Phys. Rep.* **58** 1
[26] Thorne A, Litzen U and Johansson S 1999 *Spectrophysics* (Berlin: Springer)
[27] Unsold A 1955 *Physik der Sternatmospharen* (Berlin: Springer)
[28] Bethe H A and Salpeter E E 1977 *Quantum Mechanics of One- and Two-Electron Atoms* (New York: Plenum)
[29] Dygdala R S, Lisicki E and Szudy J 1987 *J. Phys. B: At. Mol. Phys.* **20** 3001
[30] Cowan R D 1981 *The Theory of Atomic Structure and Spectra* (Berkeley, CA: University of California Press) and Cowan computer programs RCN, RCN2, RCG, and RCE http://plasma-gate.weizmann.ac.il/∼fnralch/rcn.html
[31] Sansonetti J E, Martin W C and Young S L 2005 *Handbook of Basic Atomic Spectroscopic Data (version 1.1.2)* (Gaithersburg, MD: National Institute of Standards and Technology) http://physics.nist.gov/Handbook
[32] Hindmarsh W R, Petford A D and Smith G 1967 *Proc. R. Soc.* A **297** 296
[33] Wilson A D and Shimoni Y 1975 *J. Phys. B: At. Mol. Opt. Phys.* **8** 2415
[34] Lewis E L 1967 *Proc. Phys. Soc.* **92** 817
[35] Gibson N D and Risley J S 1995 *Phys. Rev.* A **52** 4451
[36] Doery M R, Vredenbregt E J D, Tempelaars J G C, Beijerinck H C W and Verhaar B J 1998 *Phys. Rev.* A **57** 3603
[37] Li H H 2006 private communication